1. Supplementary marterials

1.1. *Videos of the raw HSPIV image, instantaneous and ensemble average velocity fields*

For the illustration of the swash flow, the complete sets of the raw images and the instantaneous velocity fields for NB12, NB45, SB12, and SB45 are presented in the videos as follows:
(1) movie1. Movie of the raw HSPIV images for NB12.
(2) movie2. Movie of the instantaneous velocity fields for NB12 corresponding to movie1.
(3) movie3. Movie corresponding to figure 3 left column: Raw HSPIV images for NB45.
(4) movie4. Movie corresponding to figure 3 right column: Instantaneous velocity fields for NB45.
(5) movie5. Movie of the raw HSPIV images for SB12.
(6) movie6. Movie of the instantaneous velocity fields for SB12 corresponding to movie5.
(7) movie7. Movie corresponding to figure 4 left column: Raw HSPIV images for SB45.
(8) movie8. Movie corresponding to figure 4 right column: Instantaneous velocity fields for SB45.

The corresponding ensemble-averaged velocity fields are as follows:
(1) movie9. Ensemble-averaged velocity fields for NB12.
(2) movie10. Ensemble-averaged velocity fields for NB45.
(3) movie11. Ensemble-averaged velocity fields for SB12.
(4) movie12. Ensemble-averaged velocity fields for SB45.

1.2. *HSPIV raw images and the instantaneous velocity fields for NB12 and SB12*

The first uprush-downwash interactions for both weakly interacting and strongly interacting cases (NB12 and SB12) are uniquely different from their subsequent interactions. The raw images with the conrresponding velocity fields for NB12 and SB12 are shown in figures S1 and S2. For the weakly interacting case, the major difference of NB12 from the rest of the interactions is that a strong splash up occurs during the downwash flow due to the larger runup of the first wave. This splash up can be seen on the water surface at $t/T = -0.028$ (figure S1). The eddies generated from the bed during the downwash flow can be traced by the white seeding particles between $x = -40$ cm and -35 cm in the raw image at $t/T = -0.057$ (figure S1. The evolution of the bed-generagted eddies can be seen in movie 1. For the strongly interacting case, the major difference of SB12 from the rest of the interactions is that the breaking occurs at the farthest onshore location. The plunging broken bore is not captured within the measurement area ($t/T = 0.114$ in figure S2).

1.3. *Turbulent velocity intensity profiles in the z−direction*

In order to further illustrate that the uprush-downwash interaction reaches quasi-steady state after the third wave, the vertical profiles of the turbulent velocity intensities $\sqrt{\langle u^2 \rangle}$ and $\sqrt{\langle w^2 \rangle}$ of the five interactions for the NB and SB cases are shown in figures S3 to S6. For the NB case, the maximum $\sqrt{\langle u^2 \rangle}$ is roughly twice of $\sqrt{\langle w^2 \rangle}$ (figures S3 and S4a to f). The order of magnitude of both $\sqrt{\langle u^2 \rangle}$ and $\sqrt{\langle w^2 \rangle}$ at the corresponding instant t/T are remarkably close among the five interactions even when the non-stationary hydraulic jump and broken bore happen.

For the SB case shown in figures S5 and S6, $\sqrt{\langle u^2 \rangle}$ and $\sqrt{\langle w^2 \rangle}$ are roughly the same order of magnitude (figures S5e, f and S6e, f). The profiles of $\sqrt{\langle u^2 \rangle}$ and $\sqrt{\langle w^2 \rangle}$ for SB34, SB45, and SB56 collapse not only during the downwash phases and the later uprush phases (figures S5 and S6a, b, i, and j), the profiles are very close during the plunging breaking (figures S5e, f and S6e, f).

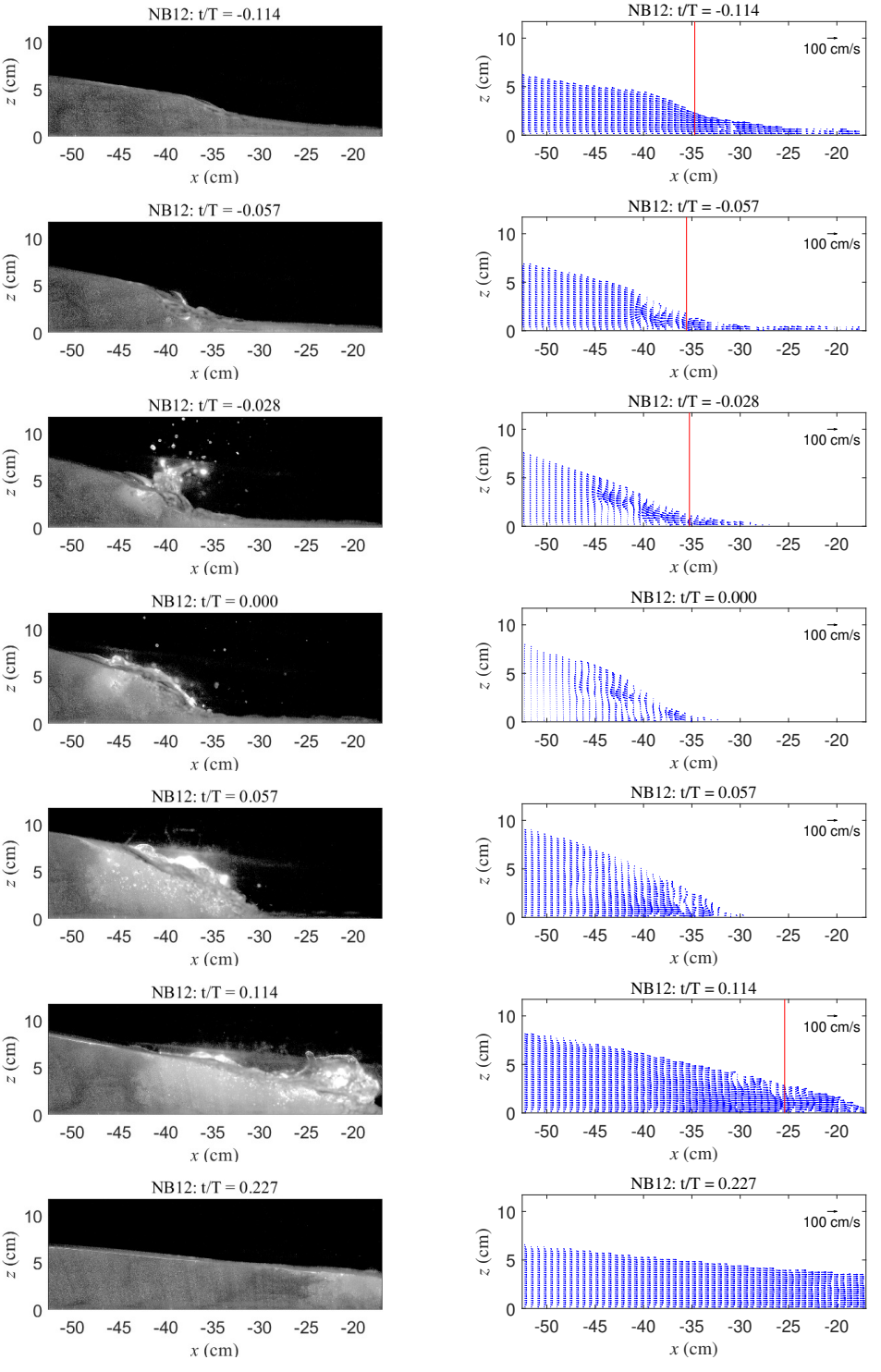

Figure S1: Raw HSPIV images (left column) and instantaneous velocity fields (right column) for NB12. The red vertical line indicates the location for the Froude number $Fr = 1$.

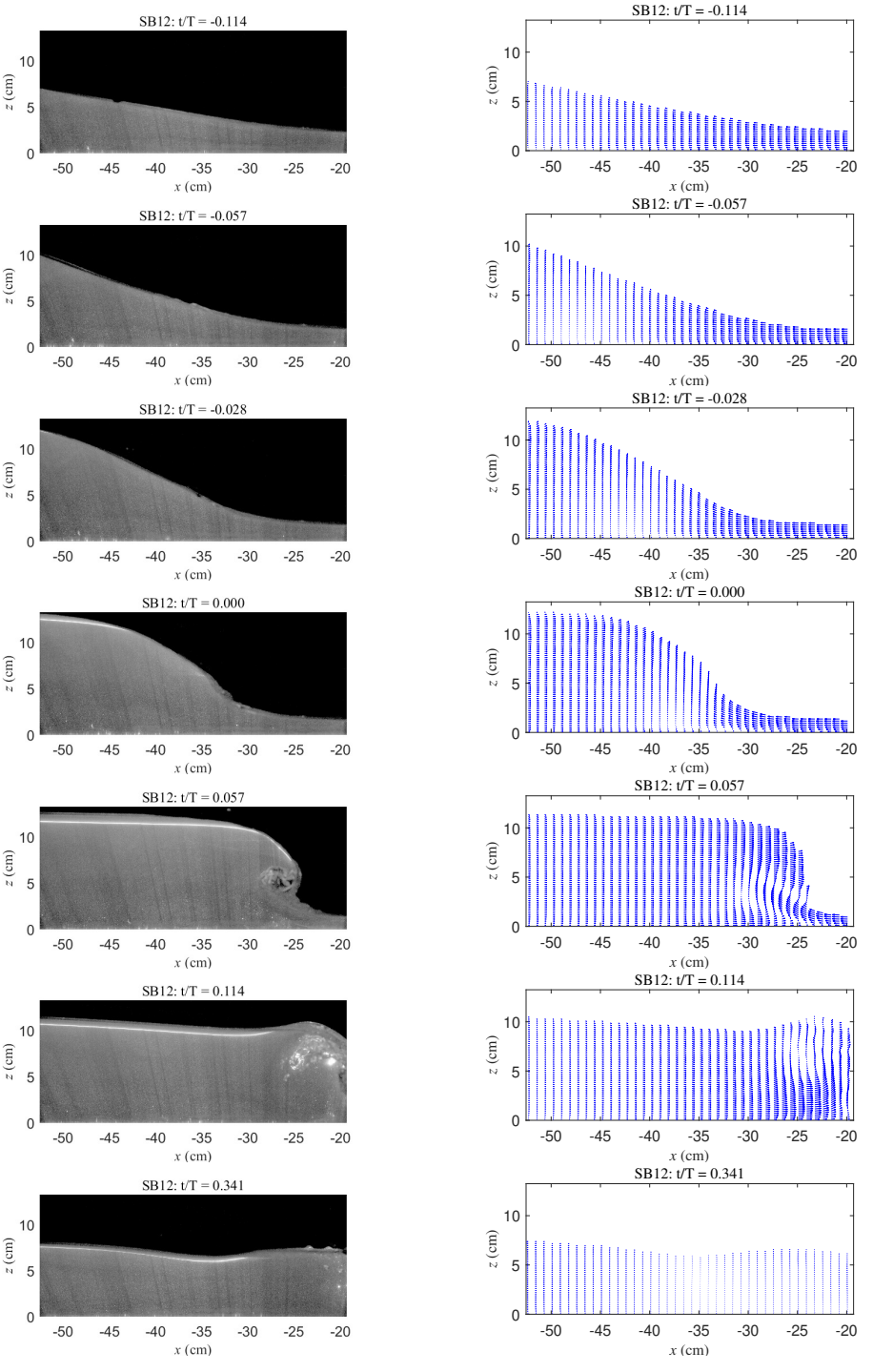

Figure S2: Raw HSPIV images (left cloumn) and instantaneous velocity fields (right column) for SB12. The red vertical line indicates the location for the Froude number $Fr = 1$

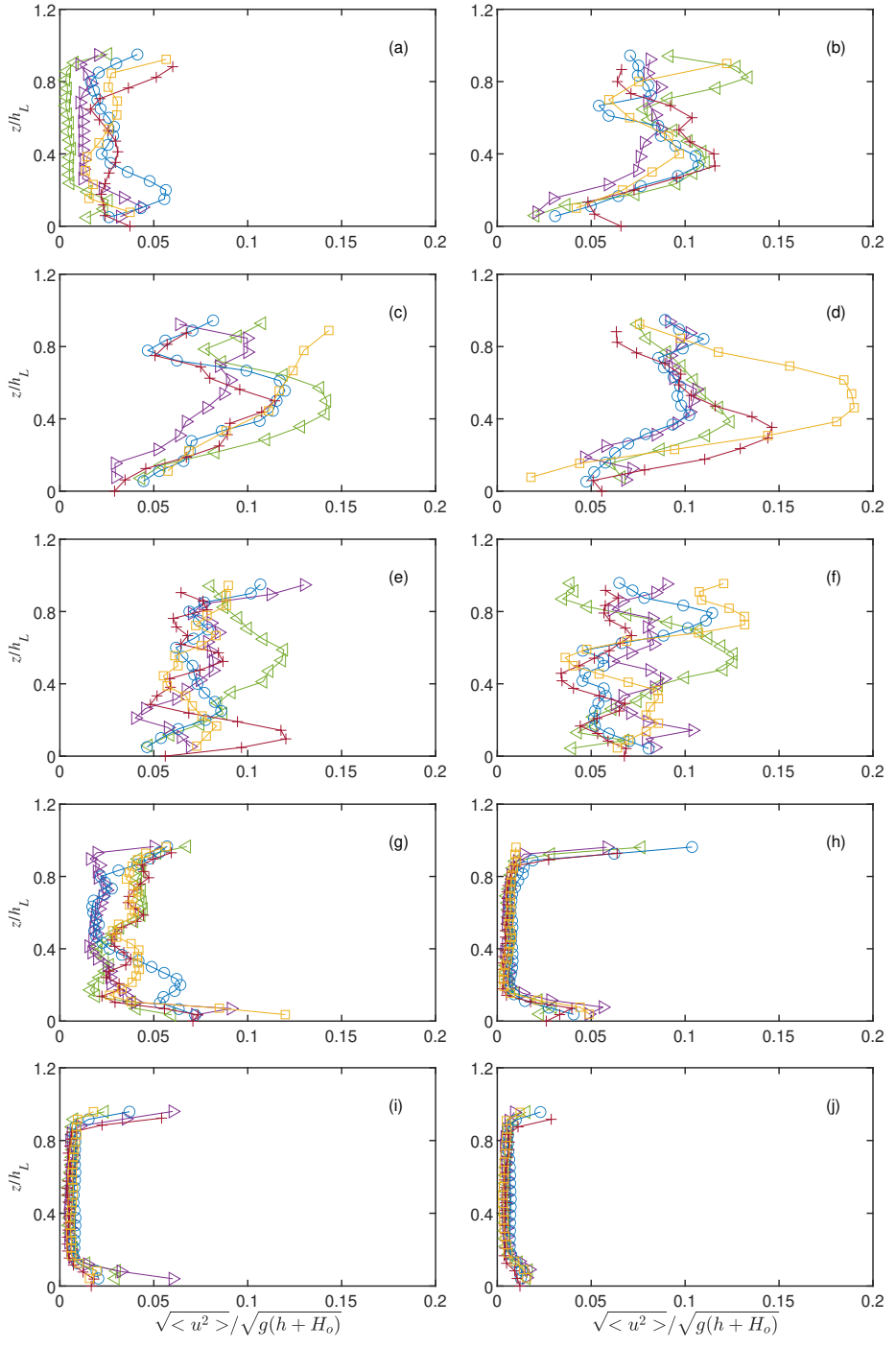

Figure S3: Snapshots of the vertical profiles of the turbulence intensity, $\sqrt{\langle u^2 \rangle}$, for the interaction NB12(◁ ◁ ◁), NB23(▷ ▷ ▷), NB34(○ ○ ○), NB45(+ + +), and NB56(□□□) at $x = -39.21$ cm. t/T = (a) -0.114, (b) -0.057, (c) -0.028, (d) 0.000, (e) 0.028, (f) 0.057, (g) 0.114, (h) 0.227, (i) 0.284, (j) 0.341.

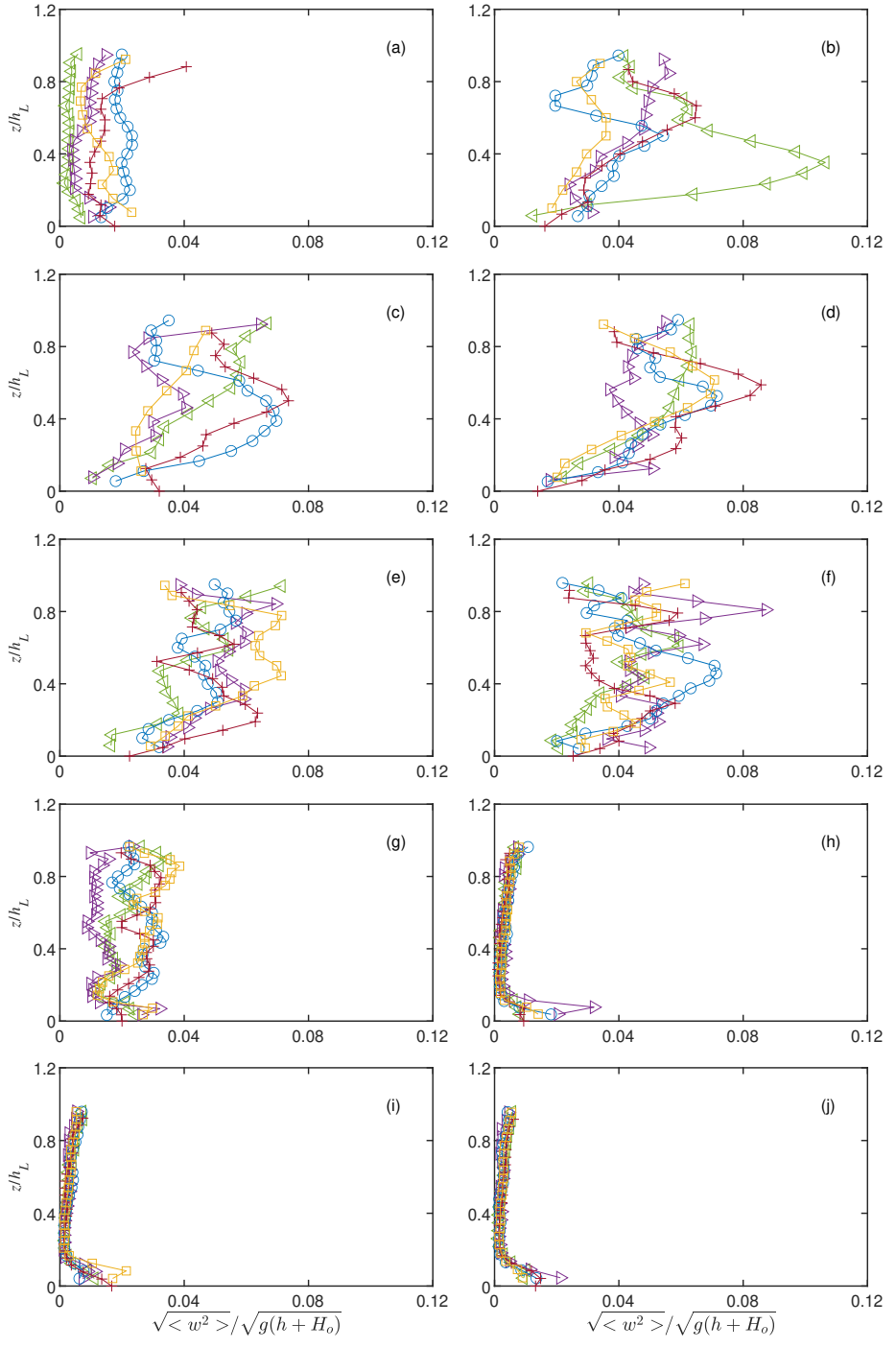

Figure S4: Snapshots of the vertical profiles of the turbulence intensity, $\sqrt{\langle w^2 \rangle}$, for the interaction NB12(◁ ◁ ◁), NB23(▷ ▷ ▷), NB34(○ ○ ○), NB45(+ + +), and NB56(□□□) at $x = -39.21$ cm. The snapshots were taken at the same instants as those shown in figure S3.

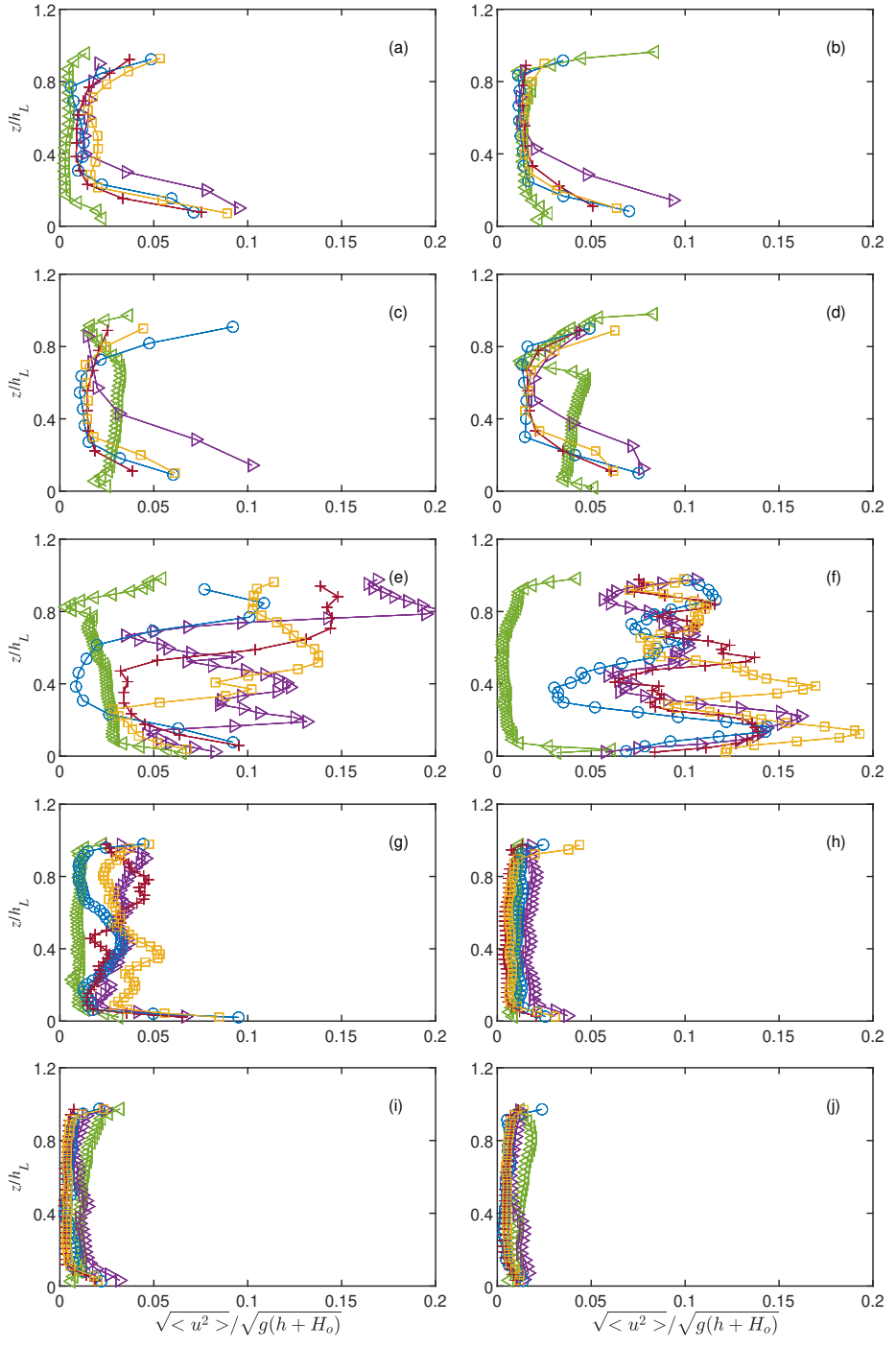

Figure S5: Snapshots of the vertical profiles of the turbulence intensity, $\sqrt{\langle u^2 \rangle}$, for the interaction SB12(◁ ◁ ◁), SB23(▷ ▷ ▷), SB34(○ ○ ○), SB45(+ + +), and SB56(□□□) at $x = -40.08$ cm. The snapshots were taken at the same instants as those shown in figure S3.

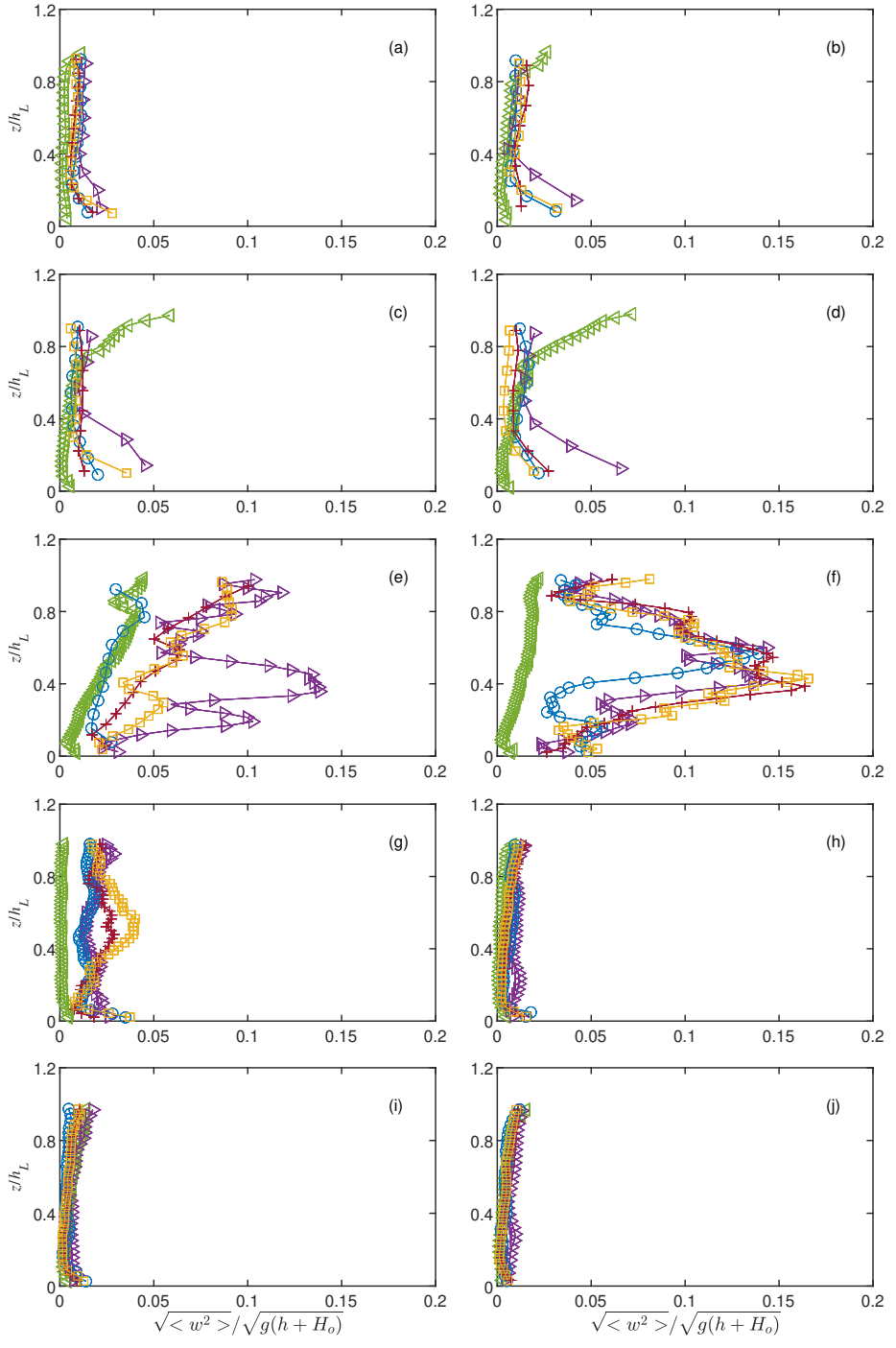

Figure S6: Snapshots of the vertical profiles of the turbulence intensity, $\sqrt{\langle w^2 \rangle}$, for the interaction SB12(◁ ◁ ◁), SB23(▷ ▷ ▷), SB34(○ ○ ○), SB45(+ + +), and SB56(□□□) at $x = -40.08$ cm. The snapshots were taken at the same instants as those shown in figure S3.